ACS OMEGA

Open Access

http://pubs.acs.org/journal/acsodf

Article

Synthesis and Structure−Activity Relationship of Phosphonate Esters with (*S*)-Cinerolone and (*S*)-Jasmololone as Irreversible Inhibitors of the GDSL Esterase/Lipase TcGLIP to Study Pyrethrin Biosynthesis

Takato Kurosawa,[⊥] Noritada Matsuo,[⊥] Keisuke Takemoto,[⊥] Akari Murai, Makoto Ihara, Yoo Tanabe, and Kazuhiko Matsuda*

Cite This: *ACS Omega* 2025, 10, 19436−19443

Read Online

ACCESS | Metrics & More | Article Recommendations | Supporting Information

ABSTRACT: TcGLIP, a GDSL esterase/lipase family enzyme found widely across species, synthesizes natural insecticides pyrethrins with (1*R*,3*R*)-chrysanthemoyl CoA and (*S*)-rethrolones as substrates in the Dalmatian Daisy *Tanacetum cinerariifolium*. We previously reported that alkyl- or benzyl-substituted phosphonate esters with (*S*)-pyrethrolone blocked TcGLIP at nanomolar ranges, but the mechanism of enzyme−substrate interactions remains elusive. Notably, it is unclear whether the conjugated diene of (*S*)-pyrethrolonyl moiety is essential for TcGLIP inhibition and whether such probes are effective in blocking pyrethrin biosynthesis for other pyrethrum plant species capable of cinerin I/II and jasmolin I/II biosynthesis but not pyrethrin I/II. In this study, *n*-pentyl- or *n*-octyl-substituted phosphonate esters were synthesized with either (*S*)-cinerolone or (*S*)-jasmololone lacking the conjugated diene as mixtures of $(S)_p$, $(S)_c$ and $(R)_p$, $(S)_c$ diastereomers, then TcGLIP inhibition was evaluated. These compounds blocked TcGLIP in the order of (*S*)-pyrethrolonyl > (*S*)-cinerolonyl > (*S*)-jasmololonyl esters regardless of whether the alkyl chain moiety was *n*-pentyl or *n*-octyl. The $(S)_p$, $(S)_c$ isomers were more potent inhibitors than the corresponding $(R)_p$, $(S)_c$ isomers for the *n*-pentyl series compounds. In contrast, the inverse was the case for the *n*-octyl series compounds. These results contribute to understanding TcGLIP recognition mechanisms of the rethrolone alkyl chain and phosphorus atom and assist in probe design to influence pyrethrin biosynthesis in Asteraceae plants.

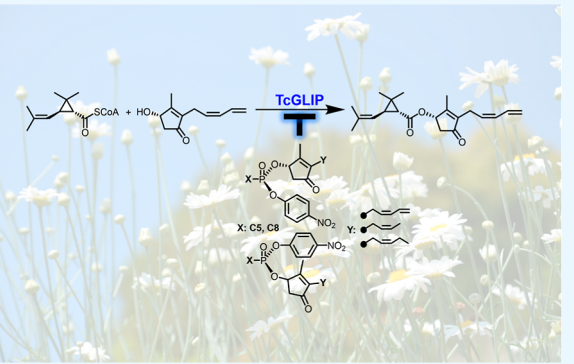

INTRODUCTION

Pyrethrins are natural insecticides produced by the Dalmatian Daisy *Tanacetum cinerariifolium* and related Asteraceae plant species.[1−5] Six compounds are generated in flowers and leaves by esterification of two kinds of acids [(1*R*,3*R*)-chrysanthemic acid and (1*R*,3*R*)-pyrethric acid] and three kinds of cyclopentenone alcohols [(*S*)-pyrethrolone, (*S*)-cinerolone, and (*S*)-jasmololone] (Figure 1A). Pyrethrins are well-known to modify voltage-gated sodium channels, inducing repetitive insect nervous system firing, quickly knocking down flying insects such as mosquitoes and house flies.[6] However, recent studies also identified pyrethrin modulation of odorant receptors in antennae sensilla, repelling flying insects.[7,8]

Given the increasing demand for nonpersistent pyrethrins, improving *T. cinerariifolium* pyrethrin productivity is critical. To this end, pyrethrin biosynthesis was partially clarified,[1] with identification and characterization of some enzymes involved in biosynthesis.[2,3,5,9−13] Also, studies revealed that mechanical wounding of plants and associated volatile wound-induced signals enhanced pyrethrin biosynthesis.[14−16] We identified the enzyme TcGLIP (Figure 1B), a GDSL esterase/lipase underpinning the ester-forming process in pyrethrin biosynthesis.[2] TcGLIP shows high substrate specificity, recognizing natural substrate absolute configurations. TcGLIP also exhibits catalytic efficiency in the order of (*S*)-pyrethrolone > (*S*)-cinerolone, (*S*)-jasmololone in accordance with the contents in *T. cinerariifolium* of pyrethrins > cinerins, jasmolins, suggesting a key role for TcGLIP in pyrethrin biosynthesis.[17]

To further understand the pyrethrin biosynthesis mechanism, we previously created a series of phosphonate probes containing the (*S*)-pyrethrolonyl moiety as irreversible TcGLIP inhibitors (Figure 2).[18] We found that, among the series of compounds, the phosphonate probes with *n*-pentyl

Received: December 4, 2024
Revised: March 25, 2025
Accepted: April 8, 2025
Published: May 9, 2025

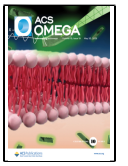

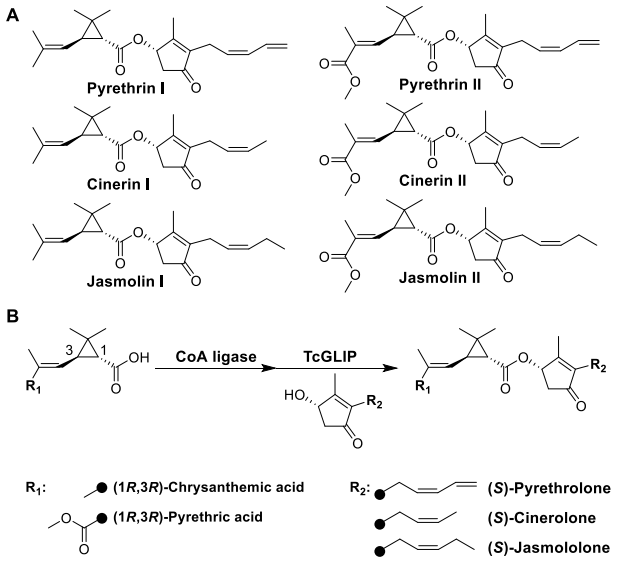

Figure 1. Six pyrethrins (A) and GDSL esterase/lipase TcGLIP that catalyzes pyrethrin ester bond formation via an acyltransferase reaction (B).

and (*S*)-pyrethrolonyl moieties (Figure 2, **1a**) most strongly inhibited the enzyme, suppressing pyrethrin biosynthesis in vivo. However, the importance of the conjugated diene in **1a** with the $(S)_p$, $(S)_c$ configurations for TcGLIP interactions is uncertain. Additionally, **1a** may not the best probe with which to study pyrethrin biosynthesis in species other than *T. cinerariifolium* if they lack (*S*)-pyrethrolone biosynthesis capacity. Therefore, we synthesized novel phosphonates with (*S*)-cinerolonyl (**2a**, **2b**, **5a**, **5b**) and (*S*)-jasmololonyl moieties (**3a**, **3b**, **6a**, **6b**) lacking the diene (Figure 2) and investigated the structure−activity relationships involving TcGLIP inhibition for **1a**−**6a** and **1b**−**6b**.

RESULTS AND DISCUSSION

We report the first synthesis of the *n*-pentyl or *n*-octyl substituted, 4-nitrophenyl phosphonate esters of (*S*)-cinerolone and (*S*)-jasmololone by the one-pot sequential reaction of *n*-pentylphosphoryl or *n*-octylphosphoryl dichloride with the rethrolone alcohol, then with 4-nitrophenol. Initial reaction of the dichloride with 4-nitrophenol followed by the rethrolone alcohol afforded no substantial yield of the desired product, likely due to structural bulkiness of the mono-4-nitrophenylated phosphorus which hindered nucleophilic attack of the rethrolone secondary hydroxy group. The resultant mixture of diastereomers was separated by silica gel (SiO_2 gel) column chromatography using an *n*-hexane/ethyl acetate (EtOAc) eluant. Previously, the R_f values on SiO_2 gel TLC for phosphonate esters with (*S*)-pyrethrolone were found to be well-resolved from high polarity to low in a hexane/EtOAc system for $(S)_p$, $(S)_c$ and $(R)_p$, $(S)_c$ configurations.[18] According to this, we assigned the absolute configurations of the phosphonates incorporating (*S*)-cinerolone and (*S*)-jasmololone (see Supporting Information Figures S1−S12 for NMR spectra).

TcGLIP inhibition activity was determined in terms of pIC_{50} [$-\log IC_{50}$ (M)] for **1a**−**6a** and **1b**−**6b** from the concentration-inhibition data (Figure 3). The pIC_{50} values of **1a**, **1b**, **4a**, and **4b** were not significantly different from those determined previously,[18] confirming enzyme inhibition assay reproducibility. Of the *n*-pentyl probes, **1a** with (*S*)-pyrethrolonyl and *n*-pentyl moieties was more potent in pIC_{50} than both **2a** with cinerolonyl moiety (7.53) and **3a** containing the (*S*)-jasmololonyl moiety (7.39). Similarly, **1b** yielded a higher pIC_{50} value than **2b** and **3b** (Table 1), demonstrating the greater affinity of TcGLIP for the conjugated diene in (*S*)-pyrethrolone over the corresponding methyl group in (*S*)-cinerolone and the ethyl group in (*S*)-jasmololone.[17] Interestingly, compounds with $(S)_p$, $(S)_c$ configuration (**1a**−**3a**) more potently inhibited TcGLIP than corresponding compounds with $(R)_p$, $(S)_c$ configuration (**1b**−**3b**) for the C5 series, whereas compounds with $(R)_p$, $(S)_c$ configuration (**4b**−**6b**) yielded higher inhibitory activities than corresponding compounds with $(S)_p$, $(S)_c$ configuration for the *n*-octyl series (**4a**−**6a** vs **4b**−**6b**). These results reflect the two-step reaction mechanism where (1*R*,3*R*)-chrysanthemoyl CoA first accesses the binding site for acyl transfer to Ser40, locating the bulky CoA outside the enzyme, and next (*S*)-pyrethrolone attacks the (1*R*,3*R*)-chrysanthemoylated Ser40 carbonyl carbon yielding pyrethrin I.[18] This data points to a mechanism in which TcGLIP recognition of the side chain in the rethrolonyl moiety occurs independently, rather than synergistically, to the binding of the *n*-alkyl chain and phosphorus atom.

We previously showed that **1a** not only blocked TcGLIP but also suppressed pyrethrin levels in *T. cinerariifolium* seedlings, whereas **1b** was ineffective in vivo. Therefore, **1a** is more useful than **1b** for studying pyrethrin biosynthesis in *T. cinerariifolium*. However, in other Asteraceae plant species, pyrethrin biosynthesis may not be inhibited efficiently by **1a** if the capacity to biosynthesize (*S*)-pyrethrolone is absent. In such cases, **2a** and **3a** may be employed to identify missing factors in pyrethrin biosynthesis. Additionally, each probe produced here can be used to understand mechanisms of catalysis and substrate recognition by elucidating the X-ray crystal structures of phosphonylated TcGLIP.

To examine the mechanism underlying the observed phosphonate probes' structure−activity relationships, we modeled phosphonylated TcGLIP. Phosphonylation results from nucleophilic attack by Ser40 of the phosphorus in **1a** and **4b** (Figure 4A,B). These models revealed that the C5 and C8 alkyl chains dock with distinct enzyme cavities. In contrast, the diene side chain of (*S*)-pyrethrolonyl moiety interacts with aromatic residues at the cavity inlet. Given this, the conjugated diene of (*S*)-pyrethrolonyl group likely participates more strongly in $\pi-\pi$ interactions with the aromatic rings compared to the side chains of (*S*)-jasmololonyl and (*S*)-cinerolonyl groups, which have only a single double bond, yielding the observed TcGLIP inhibition activity order (Table 1). Nevertheless, in-depth structural studies are required to fully evaluate probe interactions with TcGLIP.

In conclusion, we report for the first time the activity of the (*S*)-pyrethrolonyl moiety over the (*S*)-cinerolonyl and (*S*)-jasmololonyl moieties in the TcGLIP-inhibiting phosphonate probes regardless of the alkyl moiety being *n*-pentyl or *n*-octyl and whether the phosphorus absolute configuration is either $(S)_p$ or $(R)_p$. These results assist in designing superior TcGLIP inhibitors to better understand pyrethrin biosynthesis and its regulatory factors.

METHODS

Reagents. All reagents, including solvents for NMR analyses, were used without further purification.

https://doi.org/10.1021/acsomega.4c11003
ACS Omega 2025, 10, 19436−19443

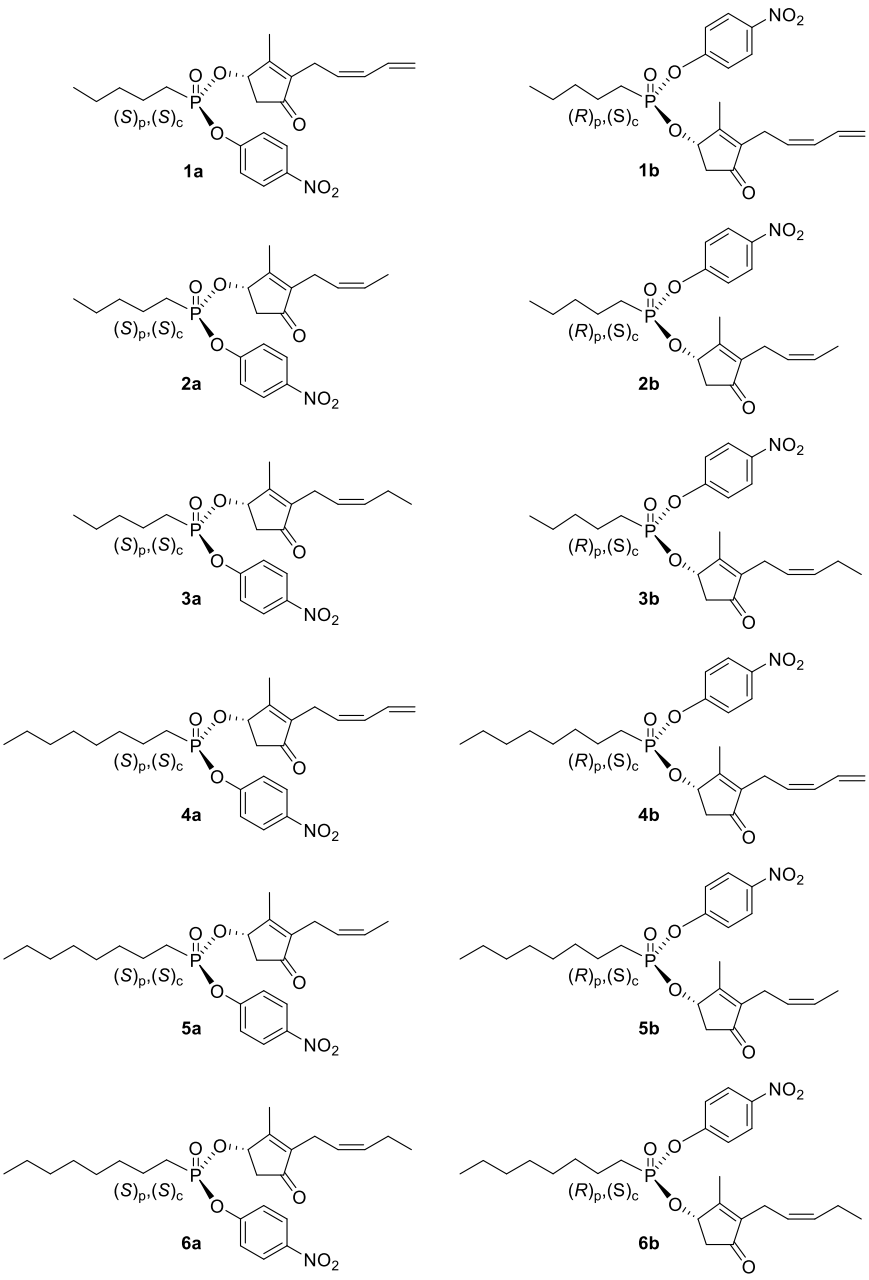

Figure 2. Phosphonate TcGLIP inhibition probes, **1a**, **1b**, **4a**, and **4b** were previously synthesized.[18]

Instruments. Optical rotation was measured using a DIP-370 (JASCO, Japan). NMR spectra were recorded using a RESONANCE ECX-500 spectrometer (JEOL, Japan) or an AVANCE III 400 spectrometer (Bruker Biospin, Germany). High-resolution mass (HRMS) spectra were measured using a Q-Tof Premier MS spectrometer (Waters, USA).

Synthesis of Compounds. All phosphonates were synthesized as described.[18] Briefly, an *n*-alkylphosphoryl dichloride was initially reacted with (*S*)-rethrolone, then with 4-nitrophenol. The resultant $(S)_p$, $(S)_c$ and $(R)_p$, $(S)_c$ diastereomers were separated by SiO_2 gel column chromatography using a hexane/EtOAc eluant.

$(S)_p$, $(S)_c$-2-Methyl-4-oxo-3-((*Z*)-2-buten-1-yl)-cyclopent-2-en-1-yl 4-Nitrophenyl *n*-Pentylphosphonate (2a); $(R)_p$, $(S)_c$-2-Methyl-4-oxo-3-((*Z*)-2-buten-1-yl)-cyclopent-2-en-1-yl 4-Nitrophenyl *n*-Pentylphosphonate (2b).

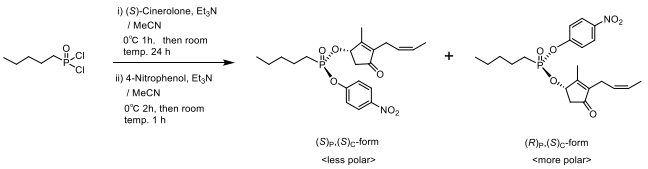

A solution of (*S*)-cinerolone (71 mg, 0.43 mmol) and Et_3N (95 mg, 0.94 mmol) in acetonitrile (MeCN) (1 mL) was added to a stirred solution of *n*-pentylphosphonic dichloride (126 mg, 0.67 mmol) in MeCN (2.5 mL) at 0−5 °C, and the mixture stirred at 0−5 °C for 1 h then at room temperature for 20 h. After TLC confirmation of complete reaction with (*S*)-cinerolone, a solution of 4-nitrophenol (167 mg, 1.20 mmol) and triethylamine (Et_3N) (97 mg, 0.96 mmol) in MeCN (2 mL) was added to the mixture at 0−5 °C, followed by stirring

https://doi.org/10.1021/acsomega.4c11003
ACS Omega 2025, 10, 19436−19443

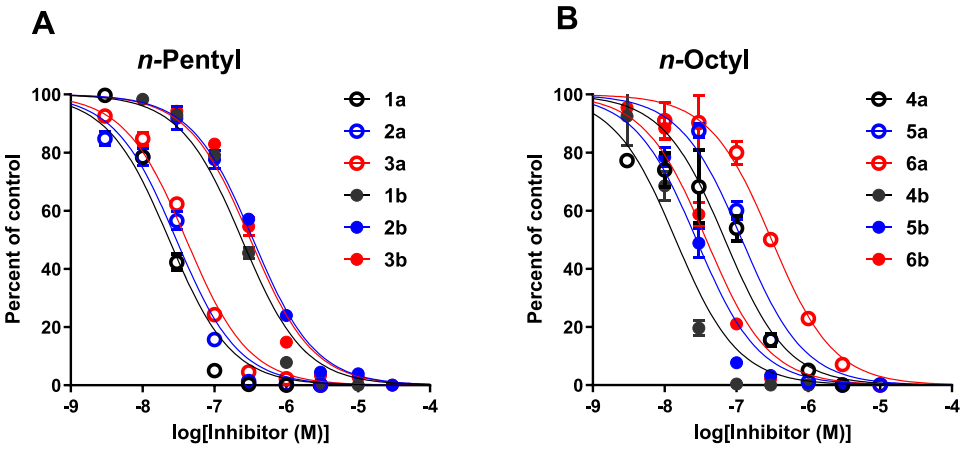

Figure 3. Concentration-TcGLIP inhibition relationships of **1a**−**6a** and **1b**−**6b**. (A) Data for *n*-pentyl containing compounds: (B) data for compounds with the *n*-octyl moiety. Each plot is represented as mean ± standard error of the mean (SEM) (n = 3).

Table 1. TcGLIP Inhibition Activities[a,b]

no	pIC_{50}	IC_{50} (μM)	no	pIC_{50}	IC_{50} (μM)
1a	7.63 ± 0.06[a]	23.5	**1b**	6.61 ± 0.04[A]	243
2a	7.53 ± 0.04[ab]	29.5	**2b**	6.46 ± 0.03[B]	347
3a	7.39 ± 0.03[bc]	40.7	**3b**	6.50 ± 0.04[BC]	318
4a	7.16 ± 0.09[x]	69.2	**4b**	7.85 ± 0.08[X]	14.3
5a	6.92 ± 0.07[y]	119	**5b**	7.56 ± 0.07[Y]	27.8
6a	6.51 ± 0.05[z]	309	**6b**	7.42 ± 0.04[Z]	38.2

[a]Data are shown as mean ± SEM (n = 3). [b]Differences in pIC_{50} values are compared by one-way ANOVA [false discovery rate (FDR) analysis][19] over four data sets, (**1a**−**3a**), (**1b**−**3b**), (**4a**−**6a**), and (**4b**−**6b**). Letters indicate significant differences [q (FDR-adjusted p) < 0.05].

at 0−5 °C for 2 h then at 25 °C for 1 h. To the mixture was added 1 M HCl aq. solution, which was then extracted twice with EtOAc. The combined organic phase was washed with brine, dried over anhydrous $MgSO_4$, and concentrated. The crude material was then purified by SiO_2 gel column chromatography (Merck 9385, stepwise shift of the composition of *n*-hexane/EtOAc mixture from 3/1 to 2/1) yielding **2a** (less polar; 15.2 mg, 8.4%) and **2b** (more polar; 13.6 mg, 7.5%).

*$(S)_p$, $(S)_c$-2-Methyl-4-oxo-3-((Z)-2-buten-1-yl)cyclopent-2-en-1-yl 4-Nitrophenyl n-Pentylphosphonate (**2a**).*

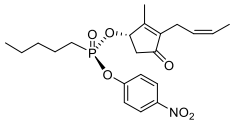

Pale yellow oil. R_f = 0.37 (*n*-hexane/EtOAc = 2/1, developed two times). HRMS (m/z): obsd 444.1547, calcd 444.1552 for $C_{21}H_{28}NO_6PNa$. $[\alpha]_D^{22}$ +42.1 (c 0.15, $CHCl_3$). ^1H NMR (500 MHz, $CDCl_3$): δ 0.91 (t, J = 7.5 Hz, 3H), 1.38 (m, 4H), 1.70 (dd, J = 7.0 Hz, 1.0 Hz, 3H), 1.72 (m, 2H), 1.99 (m, 2H), 2.12 (s, 3H), 2.34 (dd, J = 18.5 Hz, 1.5 Hz, 1H), 2.68 (dd, J = 18.5 Hz, 6.5 Hz, 1H), 2.98 (d, J = 7.0 Hz, 2H), 5.27 (m, 1H), 5.51 (m, 2H), 7.41 (d, J = 9.2 Hz, 2H).8.25 (d, J = 9.2 Hz, 2H). ^{13}C NMR (125 MHz, $CDCl_3$): δ 12.9, 13.8, 13.9, 21.1, 22.0, 22.1, 26.2 (J = 138.4 Hz), 32.6 (J = 18.0 Hz), 42.2, 75.3 (J = 7.1 Hz), 120.9 (J = 4.9 Hz), 125.1, 125.9, 125.9, 143.4, 144.7, 155.6 (J = 7.1 Hz), 164.0 (J = 7.1 Hz), 202.6. ^{31}P NMR (202 MHz, $CDCl_3$): δ 31.98.

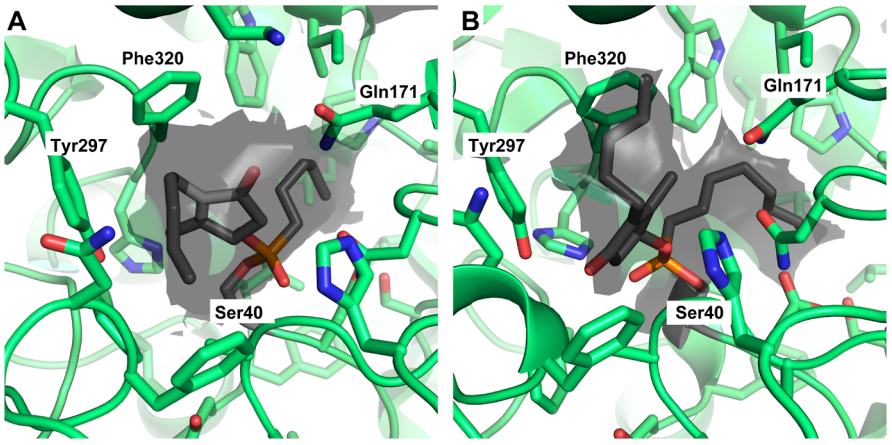

Figure 4. TcGLIPs phosphonylated by **1a** (A) and **4b** (B). Main chains of TcGLIP are colored in light green, while carbon, nitrogen, oxygen, and phosphorus atoms are colored in dark gray, blue, red, and orange, respectively. TcGLIP binding clefts for the compounds are colored transparent gray. Note the aromatic residues located close to the (*S*)-pyrethrolonyl moiety conjugated diene, explaining the structure−activity relationship shown in Table 1.

https://doi.org/10.1021/acsomega.4c11003
ACS Omega 2025, 10, 19436−19443

*$(R)_p$, $(S)_c$-2-Methyl-4-oxo-3-((Z)-2-buten-1-yl)cyclopent-2-en-1-yl 4-Nitrophenyl n-Pentylphosphonate (**2b**).*

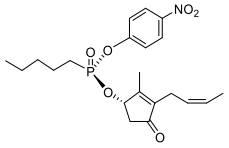

Pale yellow oil. R_f = 0.30 (*n*-hexane/EtOAc = 2/1, developed two times). HRMS (*m*/*z*): obsd 444.1555, calcd 444.1552 for $C_{21}H_{28}NO_6PNa$. $[\alpha]_D^{22}$ −31.2 (*c* 0.14, $CHCl_3$). ^1H NMR (500 MHz, $CDCl_3$): δ 0.91 (t, *J* = 7.5 Hz, 3H), 1.38 (m, 4H), 1.67 (m, 2H), 1.69 (dd, *J* = 7.0 Hz, 1.5 Hz, 3H), 1.92 (s, 3H), 1.97 (m, 2H), 2.49 (dd, *J* = 18.5 Hz, 1.5 Hz, 1H), 2.89 (dd, *J* = 18.5 Hz, 6.5 Hz, 1H), 2.97 (d, *J* = 7.0 Hz, 2H), 5.26 (m, 1H), 5.45 (dd, *J* = 7.0 Hz, 1.5 Hz, 1H), 5.51 (m, 1H), 7.45 (dd, *J* = 9.0 Hz, 1.0 Hz, 2H), 8.26 (d, *J* = 9.0 Hz, 2H). ^{13}C NMR (125 MHz, $CDCl_3$): δ 12.9, 13.8, 13.9, 21.1, 21.9, 22.0, 22.1, 26.5 (*J* = 138.3 Hz), 32.6 (*J* = 17.9 Hz), 42.5, 76.0 (*J* = 6.0 Hz), 121.1 (*J* = 4.8 Hz), 125.1, 125.8, 125.9, 143.5, 144.8, 155.6 (*J* = 8.4 Hz), 163.8 (*J* = 7.1 Hz), 202.6. ^{31}P NMR (202 MHz, CDCl3): δ 31.68.

$(S)_p$, $(S)_c$-2-Methyl-4-oxo-3-((*Z*)-2-penten-1-yl)-cyclopent-2-en-1-yl 4-Nitrophenyl *n*-Pentylphosphonate (3a); $(R)_p$, $(S)_c$-2-Methyl-4-oxo-3-((*Z*)-2-penten-1-yl)cyclopent-2-en-1-yl 4-Nitrophenyl *n*-Pentylphosphonate (3b).

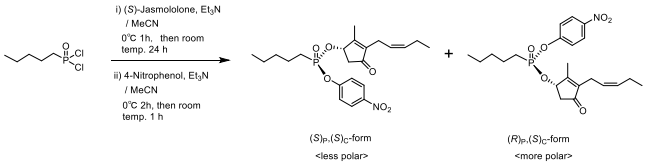

A solution of (*S*)-jasmololone (97 mg, 0.54 mmol) and Et_3N (121 mg, 1.20 mmol) in MeCN (1 mL) was added to a stirred solution of pentylphosphonic dichloride (146 mg, 0.77 mmol) in MeCN (2.5 mL) at 0−5 °C, with the mixture stirred at 0−5 °C for 1 h, then at room temperature for 22 h. A solution of 4-nitrophenol (195 mg, 1.40 mmol) and Et_3N (117 mg, 1.16 mmol) in MeCN (1.5 mL) was added to the mixture at 0−5 °C, followed by stirring at 0−5 °C for 2 h, then at 25 °C for 1 h. To the mixture was added aq. 1 M HCl solution, which was then extracted with EtOAc. The combined organic phase was washed with brine, dried over anhydrous $MgSO_4$, and concentrated. The resultant crude was purified by SiO_2 gel column chromatography (Merck 9385, stepwise shift of the composition of *n*-hexane/EtOAc mixture from 3/1 to 2/1) to yield **3a** (47.0 mg, 20.0%) and **3b** 38.2 mg, 16.3%).

*$(S)_p$, $(S)_c$-2-Methyl-4-oxo-3-((Z)-2-penten-1-yl)cyclopent-2-en-1-yl 4-Nitrophenyl n-Pentylphosphonate (**3a**).*

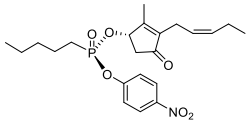

Pale yellow oil. R_f = 0.41 (*n*-hexane/EtOAc = 2/1, developed two times). HRMS (*m*/*z*): obsd 458.1708, calcd 458.1708 for $C_{22}H_{30}NO_6PNa$. $[\alpha]_D^{22}$ +40.0 (*c* 0.11, $CHCl_3$). ^1H NMR (500 MHz, $CDCl_3$): δ 0.91 (t, *J* = 7.5 Hz, 3H), 0.99 (t, *J* = 7.5 Hz, 3H), 1.35 (m, 2H), 1.42 (m, 2H), 1.71 (m, 2H), 1.98 (m, 2H), 2.11 (s, 3H), 2.14 (m, 2H), 2.34 (dd, *J* = 18.5 Hz, 1.5 Hz, 1H), 2.65 (dd, *J* = 18.5 Hz, 6.5 Hz, 1H), 2.97 (d, *J* = 7.0 Hz, 2H), 5.22 (m, 1H), 5.43 (m, 1H), 5.48 (m, 1H), 7.39 (dd, *J* = 9.0 Hz, 1.5 Hz, 2H), 8.23 (d, *J* = 9.0 Hz, 2H). ^{13}C NMR (125 MHz, $CDCl_3$): δ 13.7, 13.8, 14.0, 20.6, 21.3, 21.9 (*J* = 4.8 Hz), 22.0, 26.3 (*J* = 138.4 Hz), 32.5 (*J* = 16.6 Hz), 42.2, 75.4 (*J* = 7.1 Hz), 120.9 (*J* = 4.8 Hz), 123.5, 125.7, 133.6, 143.5, 144.9, 155.6 (*J* = 8.3 Hz), 163.5 (*J* = 7.1 Hz), 202.1. ^{31}P NMR (202 MHz, $CDCl_3$): δ 31.73.

*$(R)_p$, $(S)_c$-2-Methyl-4-oxo-3-((Z)-2-penten-1-yl)cyclopent-2-en-1-yl 4-Nitrophenyl n-Pentylphosphonate (**3b**).*

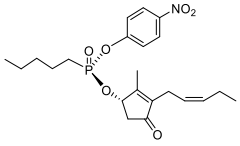

Pale yellow oil. R_f = 0.35 (*n*-hexane/EtOAc = 2/1, developed two times). HRMS (*m*/*z*): obsd 458.1709, calcd 458.1708 for $C_{22}H_{30}NO_6PNa$. $[\alpha]_D^{22}$ −29.7 (*c* 0.15, $CHCl_3$); ^1H NMR (500 MHz, $CDCl_3$): δ 0.91 (t, *J* = 7.5 Hz, 3H), 0.98 (t, *J* = 7.5 Hz, 3H), 1.37 (m, 4H), 1.68 (m, 2H), 1.92 (s, 3H), 1.97 (m, 2H), 2.13 (m, 2H), 2.49 (dd, *J* = 18.5 Hz, 2.0 Hz, 1H), 2.89 (dd, *J* = 18.5 Hz, 6.5 Hz, 1H), 2.96 (d, *J* = 7.5 Hz, 2H), 5.20 (m, 1H), 5.42 (m, 1H), 5.44 (m, 1H), 7.45 (dd, *J* = 9.0 Hz, 1.0 Hz, 2H), 8.26 (d, *J* = 9.0 Hz, 2H). ^{13}C NMR (125 MHz, $CDCl_3$): δ 13.7, 13.8, 14.1, 20.6, 21.2, 21.9 (*J* = 5.9 Hz), 22.1, 26.4 (*J* = 137.1 Hz), 32.5 (*J* = 17.9 Hz), 42.4, 75.9 (*J* = 7.1 Hz), 121.0 (*J* = 4.8 Hz), 123.4, 125.8, 133.5, 143.4, 144.7, 155.5 (*J* = 8.4 Hz), 163.7 (*J* = 5.9 Hz), 202.5. ^{31}P NMR (202 MHz, $CDCl_3$): δ 31.60.

$(S)_p$, $(S)_c$-2-Methyl-4-oxo-3-((*Z*)-2-buten-1-yl)-cyclopent-2-en-1-yl 4-Nitrophenyl *n*-Octylphosphonate (5a); $(R)_p$, $(S)_c$-2-Methyl-4-oxo-3-((*Z*)-2-buten-1-yl)-cyclopent-2-en-1-yl 4-Nitrophenyl *n*-Octylphosphonate (5b).

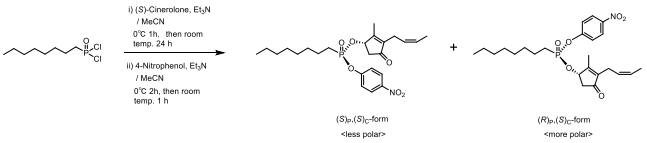

A solution of (*S*)-cinerolone (65.8 mg, 0.39 mmol) and Et_3N (109.3 mg, 1.08 mmol) in MeCN (1 mL) was added to a stirred solution of octylphosphonic dichloride (125.8 mg, 0.54 mmol) in MeCN (2.0 mL) at 0−5 °C, and the mixture stirred at 0−5 °C for 1 h then at room temperature for 20 h. A solution of 4-nitrophenol (118.6 mg, 0.85 mmol) and Et_3N (109.3 mg, 1.08 mmol) in MeCN (2 mL) was added to the mixture at 0−5 °C, followed by stirring at 0−5 °C for 2 h and at 25 °C for 1 h. Then, 1 M HCl aq. solution was added and extracted with EtOAc. The combined organic phase was washed with brine, dried over anhydrous $MgSO_4$, and concentrated. The residue was purified by SiO_2 gel column chromatography (Merck 9385, *n*-hexane/EtOAc = 3/1) to yield **5a** (8.3 mg, 3.1%) and **5b** (9.3 mg, 3.5%).

*$(S)_p$, $(S)_c$-2-Methyl-4-oxo-3-((Z)-2-buten-1-yl)cyclopent-2-en-1-yl 4-Nitrophenyl n-Octylphosphonate (**5a**).*

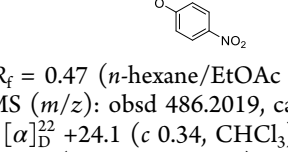

Pale yellow oil. R_f = 0.47 (*n*-hexane/EtOAc = 2/1 developed two times). HRMS (*m*/*z*): obsd 486.2019, calcd 486.2021 for $C_{21}H_{34}NO_6PNa$. $[\alpha]_D^{22}$ +24.1 (*c* 0.34, $CHCl_3$); ^1H NMR (500 MHz, $CDCl_3$): δ 0.88 (t, *J* = 6.8 Hz, 3H), 1.26 (m, 8H), 1.71 (m, 4H), 1.99 (m, 2H), 2.11 (s, 3H), 2.34 (dd, *J* = 18.4 Hz, 1.8 Hz, 1H), 2.68 (dd, *J* = 18.4 Hz, 6.4 Hz, 1H), 2.98 (d, *J* = 7.2

https://doi.org/10.1021/acsomega.4c11003
ACS Omega 2025, 10, 19436−19443

Hz, 2H), 5.27 (m, 1H), 5.51 (m, 2H), 7.41 (d, J = 9.2 Hz, 2H), 8.25 (d, J = 9.2 Hz, 2H). ^{13}C NMR (100 MHz, $CDCl_3$): δ 12.9, 13.9, 14.1, 21.0, 22.2, 22.3, 22.6, 26.2 (J = 138.5 Hz), 29.0, 30.4 (J = 17.1 Hz), 31.7, 42.1, 75.2 (J = 7.1 Hz), 120.8 (J = 4.6 Hz), 125.1, 125.8, 125.8, 143.4, 144.7, 155.5 (J = 7.8 Hz), 164.0 (J = 6.9 Hz), 202.5. ^{31}P NMR (202 MHz, $CDCl_3$): δ 31.37.

*$(R)_p$, $(S)_c$-2-Methyl-4-oxo-3-((Z)-2-buten-1-yl)cyclopent-2-en-1-yl 4-Nitrophenyl n-Octylphosphonate (**5b**).*

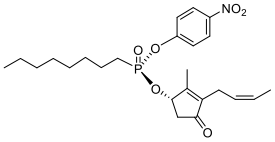

Pale yellow oil. R_f = 0.41 (n-hexane/EtOAc = 2/1, developed two times). HRMS (m/z): obsd 486.2014, calcd 486.2021 for $C_{21}H_{34}NO_6PNa$. $[\alpha]_D^{22}$ −20.7 (c 0.43, $CHCl_3$); ^{1}H NMR (500 MHz, $CDCl_3$): δ 0.88 (t, J = 7.0 Hz, 3H), 1.27 (m, 8H), 1.43 (m, 2H), 1.68 (m, 5H), 1.92 (s, 3H), 1.97 (m, 2H), 2.49 (dd, J = 18.5 Hz, 1.9 Hz, 1H), 2.89 (dd, J = 18.5 Hz, 6.3 Hz, 1H), 2.97 (d, J = 7.1 Hz, 2H), 5.26 (m, 1H), 5.45 (t, J = 6.6 Hz, 1H), 5.52 (m, 1H), 7.44 (dd, J = 9.0 Hz, 1.0 Hz, 2H), 8.26 (d, J = 9.0 Hz, 2H). ^{13}C NMR (100 MHz, $CDCl_3$): δ 12.9, 13.7, 14.1, 21.0, 22.2, 22.3, 22.6, 26.5 (J = 137.1 Hz), 26.7, 30.4 (J = 17.5 Hz), 31.7, 42.4 (J = 2.2 Hz), 75.9 (J = 6.9 Hz), 121.0 (J = 4.7 Hz), 125.1, 125.8, 125.8, 143.4, 144.7, 155.5 (J = 8.4 Hz), 163.8 (J = 6.2 Hz), 202.5. ^{31}P NMR (202 MHz, $CDCl_3$): δ 31.08.

$(S)_p$, $(S)_c$-2-Methyl-4-oxo-3-((Z)-2-penten-1-yl)-cyclopent-2-en-1-yl 4-Nitrophenyl *n*-Octylphosphonate (6a); $(R)_p$, $(S)_c$-2-Methyl-4-oxo-3-((Z)-2-penten-1-yl)-cyclopent-2-en-1-yl 4-Nitrophenyl *n*-Octylphosphonate (6b). A solution of (S)-jasmololone (77 mg, 0.43 mmol) and Et_3N (80.8 mg, 0.80 mmol) in MeCN (1 mL) was added to a stirred solution of octylphosphonic dichloride (123.1 mg, 0.53 mmol) in MeCN (2.5 mL) at 0−5 °C, and the mixture stirred at 0−5 °C for 1 h and at room temperature for 22 h. After confirming complete reaction of (S)-jasmololone by TLC, a solution of 4-nitrophenol (103.7 mg, 0.75 mmol) and Et_3N (80.8 mg, 0.80 mmol) in MeCN (2.0 mL) was added to the mixture at 0−5 °C, followed by stirring at 0−5 °C for 2 h and at 25 °C for 1 h. To the mixture was added 1 M HCl aq. solution and then extracted twice with EtOAc. The combined organic phase was washed with brine, dried over anhydrous $MgSO_4$, and concentrated. The obtained crude oil was purified by SiO_2 gel column chromatography (Merck 9385, n-hexane/EtOAc = 3/1) to give **6a** (13.18 mg, 4.7%) and **6b** (11.36 mg, 4.0%).

*$(S)_p$, $(S)_c$-2-Methyl-4-oxo-3-((Z)-2-penten-1-yl)cyclopent-2-en-1-yl 4-Nitrophenyl n-Octylphosphonate (**6a**).*

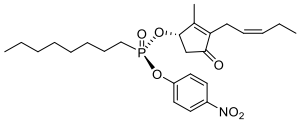

Pale yellow oil. R_f = 0.51 (n-hexane/EtOAc = 2/1, developed two times). HRMS (m/z): obsd 500.2183, calcd 500.2178 for $C_{25}H_{36}NO_6PNa$. $[\alpha]_D^{22}$ +34.8 (c 0.66, $CHCl_3$); ^{1}H NMR (400 MHz, $CDCl_3$): δ 0.89 (t, J = 7.0 Hz, 3H), 0.99 (t, J = 7.5 Hz, 3H), 1.38 (m, 8H), 1.42 (m, 2H), 1.71 (m, 2H), 1.99 (m, 2H), 2.11 (s, 3H), 2.14 (m, 2H), 2.34 (dd, J = 18.4 Hz, 2.0 Hz, 1H), 2.68 (dd, J = 18.4 Hz, 6.4 Hz, 1H), 2.98 (d, J = 7.3 Hz, 2H), 5.22 (m, 1H), 5.43 (m, 1H), 5.50 (t, J = 7.3 Hz, 1H), 7.41 (dd, J = 9.0 Hz, 1.0 Hz, 2H), 8.25 (d, J = 9.0 Hz, 2H). ^{13}C NMR (100 MHz, $CDCl_3$): δ 13.8, 14.1, 20.6, 21.2, 22.2, 22.3, 22.6, 26.2 (J = 138.5 Hz), 29.0, 30.4 (J = 17.5 Hz), 31.7, 42.1 (J = 1.1 Hz), 75.2 (J = 7.1 Hz), 120.8 (J = 4.4 Hz), 123.4, 125.8, 133.5, 143.4, 144.7, 155.5 (J = 8.0 Hz), 163.9 (J = 7.1 Hz), 202.5. ^{31}P NMR (202 MHz, $CDCl_3$): δ 31.35.

*$(R)_p$, $(S)_c$-2-Methyl-4-oxo-3-((Z)-2-penten-1-yl)cyclopent-2-en-1-yl 4-Nitrophenyl n-Octylphosphonate (**6b**).*

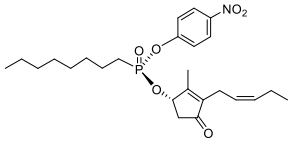

Pale yellow oil. R_f = 0.46 (n-hexane/EtOAc = 2/1, developed two times). HRMS (m/z): obsd 500.2189, calcd 500.2178 for $C_{25}H_{36}NO_6PNa$. $[\alpha]_D^{22}$ −25.7 (c 0.59, $CHCl_3$); ^{1}H NMR (400 MHz, $CDCl_3$): δ 0.88 (t, J = 7.1 Hz, 3H), 0.98 (t, J = 7.5 Hz, 3H), 1.28 (m, 8H), 1.41 (m, 2H), 1.92 (s, 3H), 1.97 (m, 2H), 2.13 (m, 2H), 2.48 (dd, J = 18.5 Hz, 2.0 Hz, 1H), 2.89 (dd, J = 18.4 Hz, 6.3 Hz, 1H), 2.96 (d, J = 7.2 Hz, 2H), 5.20 (m, 1H), 5.43 (m, 2H), 7.44 (dd, J = 9.2 Hz, 1.0 Hz, 2H), 8.26 (d, J = 9.0 Hz, 2H). ^{13}C NMR (100 MHz, $CDCl_3$): δ 13.7, 14.1, 20.6, 21.2, 22.2, 22.3, 22.6, 26.5 (J = 137.6 Hz), 29.0, 30.4 (J = 17.5 Hz), 31.7, 42.4, 75.9 (J = 6.6 Hz), 121.0 (J = 4.7 Hz), 123.4, 125.8, 133.5, 143.4, 144.7, 155.5 (J = 8.0 Hz), 163.7 (J = 6.4 Hz), 202.5. ^{31}P NMR (202 MHz, $CDCl_3$): δ 31.07.

Purity of the Compounds. Compound purity was evaluated by HPLC (Purity >95% excluding the DMSO peak; see Supporting Information Figures S13 and S14).

Expression and Purification of TcGLIP. TcGLIP fused with the maltose binding protein (MBP) was expressed in *Escherichia coli* (Origami B strain) then purified by affinity chromatography with Amylose resin (New England Biolabs, USA) and anion exchange chromatography with Mono Q resin (Cytiva, USA) as reported previously.[17,18]

TcGLIP Inhibition Assay. The purified MBP-TcGLIP (4 μg mL^{-1}) was incubated in 50 mM Tris buffer (pH 7.5) with the inhibitor for 10 min then reacted with 2 mM (1*R*,3*R*)-chrysanthemoyl CoA and 1 mM (S)-pyrethrolone for 10 min at 25 °C. The reaction was stopped by acetic acid addition and extracted with an equal volume of n-hexane. Pyrethrin I in the extract was measured using UV absorbance at 230 nm by HPLC with a Cadenza CD-C18 column (4.6 × 100 mm, Imtakt, Japan) and an 80% MeCN/20% water mixture at a flow rate of 1 mL min^{-1}.

Data Analysis. TcGLIP inhibition-concentration data were analyzed by nonlinear regression using Prism 10.2.3 (Siemens, Germany) to determine IC_{50} (M), the concentration at which activity is inhibited to half that of the control.[18] Experiments were performed in triplicate. Statistical analysis was performed using Prism 10.2.3 by one-way ANOVA (FDR) analysis[19]) at a significant level of q < 0.05.

***In silico* Modeling of TcGLIP-Inhibitor Complexes.** To model the covalently bound TcGLIP-inhibitor complexes, preliminary structures were first constructed using AutoDock 4.2 software.[20] Molecular dynamics calculations were then performed for energy minimization using Gromacs 2022.4[21] and GAFF2[22] force field with the TIP3 water model. For force field parameters of the covalently bound inhibitors, structure coordinates of the inhibitors were complexed with those of serine whose amino- and carboxy-group were blocked with acetyl and methylamine groups, respectively, and the RESP charges calculated after optimization with B3LYP/6−31G(d,p)

https://doi.org/10.1021/acsomega.4c11003
ACS Omega 2025, 10, 19436−19443

using GAMESS software version 2023R2.[23] Inhibitor force field parameters were prepared with the AmberTool24 package using a punch file from GAMESS calculations and manually edited for the TcGLIP-inhibitor system. After a steepest descent and conjugate gradient minimization, followed by *NVT* and *NPT* equilibration, each MD production run was performed for 100 ns. RMSD differences for Cα carbons were evaluated to reflect system equilibrium. Movement of Cα carbons settled after approximately 50 ns, with no subsequent significant movement of bound ligands observed. Graphical representations were prepared using the open-source version of PyMOL Molecular Graphics System, Version 2.6 (Schrödinger, USA).

■ ASSOCIATED CONTENT

Supporting Information

The Supporting Information is available free of charge at https://pubs.acs.org/doi/10.1021/acsomega.4c11003.

Figure S1. ^{1}H NMR spectra of **2a** and **2b** in $CDCl_3$
Figure S2. ^{13}C NMR spectra of **2a** and **2b** in $CDCl_3$
Figure S3. ^{31}P NMR spectra of **2a** and **2b** in $CDCl_3$
Figure S4. ^{1}H NMR spectra of **3a** and **3b** in $CDCl_3$
Figure S5. ^{13}C NMR spectra of **3a** and **3b** in $CDCl_3$
Figure S6. ^{31}P NMR spectra of **3a** and **3b** in $CDCl_3$
Figure S7. ^{1}H NMR spectra of **5a** and **5b** in $CDCl_3$
Figure S8. ^{13}C NMR spectra of **5a** and **5b** in $CDCl_3$
Figure S9. ^{31}P NMR spectra of **5a** and **5b** in $CDCl_3$
Figure S10. ^{1}H NMR spectra of **6a** and **6b** in $CDCl_3$
Figure S11. ^{13}C NMR spectra of **6a** and **6b** in $CDCl_3$
Figure S12. ^{31}P NMR spectra of **6a** and **6b** in $CDCl_3$
Figure S13. HPLC of **2a**, **2b**, **3a**, and **3b** recorded using a Cadenza CD-C18 column (4.6 × 100 mm; Imtakt, Japan) with 80% acetonitrile/water at a flow rate of 1 mL min^{-1}. *Y* axis is absorbance at 230 nm. Figure S14. HPLC of **5a**, **5b**, **6a**, and **6b** recorded using a Cadenza CD-C18 column (4.6 × 100 mm; Imtakt, Japan) with 80% acetonitrile/water at a flow rate of 1 mL min^{-1}. *Y* axis is absorbance at 230 nm (PDF)

■ AUTHOR INFORMATION

Corresponding Author

Kazuhiko Matsuda − *Graduate School of Agriculture and Department of Applied Biological Chemistry, Faculty of Agriculture, Kindai University, Nara 631-8505, Japan; Agricultural Technology and Innovation Research Institute, Kindai University, Nara 631-8505, Japan;* orcid.org/0000-0002-1299-4570; Email: kmatsuda@nara.kindai.ac.jp

Authors

Takato Kurosawa − *Graduate School of Agriculture, Kindai University, Nara 631-8505, Japan*

Noritada Matsuo − *Department of Applied Biological Chemistry, Faculty of Agriculture, Kindai University, Nara 631-8505, Japan*

Keisuke Takemoto − *Graduate School of Agriculture, Kindai University, Nara 631-8505, Japan*

Akari Murai − *Department of Applied Biological Chemistry, Faculty of Agriculture, Kindai University, Nara 631-8505, Japan*

Makoto Ihara − *Graduate School of Agriculture and Department of Applied Biological Chemistry, Faculty of Agriculture, Kindai University, Nara 631-8505, Japan;* orcid.org/0000-0002-6403-0781

Yoo Tanabe − *Department of Chemistry, School of Science and Technology, Kwansei Gakuin University, Sanda, Hyogo 669-1337, Japan;* orcid.org/0000-0003-3265-4343

Complete contact information is available at: https://pubs.acs.org/10.1021/acsomega.4c11003

Author Contributions

$^{\perp}$T.K., N.M., and K.T. contributed equally to this study.

Notes

The authors declare no competing financial interest.

■ ACKNOWLEDGMENTS

K.M. acknowledges the Kindai University for support of this study. Also, K.M. is grateful to the Agricultural Technology and Innovation Research Institute of Kindai University for support of publication in *ACS Omega*.

■ REFERENCES

(1) Matsuda, K.; Kikuta, Y.; Haba, A.; Nakayama, K.; Katsuda, Y.; Hatanaka, A.; Komai, K. Biosynthesis of pyrethrin I in seedlings of *Chrysanthemum cinerariaefolium*. *Phytochemistry* **2005**, *66* (13), 1529−1535.

(2) Kikuta, Y.; Ueda, H.; Takahashi, M.; Mitsumori, T.; Yamada, G.; Sakamori, K.; Takeda, K.; Furutani, S.; Nakayama, K.; Katsuda, Y.; Hatanaka, A.; Matsuda, K. Identification and characterization of a GDSL lipase-like protein that catalyzes the ester-forming reaction for pyrethrin biosynthesis in *Tanacetum cinerariifolium*- a new target for plant protection. *Plant J.* **2012**, *71* (2), 183−193.

(3) Li, W.; Lybrand, D. B.; Zhou, F.; Last, R. L.; Pichersky, E. Pyrethrin biosynthesis: The cytochrome P450 oxidoreductase CYP82Q3 converts jasmolone to pyrethrolone. *Plant Physiol.* **2019**, *181* (3), 934−944.

(4) Matsuo, N. Discovery and development of pyrethroid insecticides. *Proc. Jpn. Acad. Ser. B Phys. Biol. Sci.* **2019**, *95* (7), 378−400.

(5) Matsuda, K. Understanding pyrethrin biosynthesis: toward and beyond natural pesticide overproduction. *Biochem. Soc. Trans.* **2024**, *52* (4), 1927−1937.

(6) Narahashi, T. Nerve membrane ion channels as the target site of insecticides. *Mini Rev. Med. Chem.* **2002**, *2* (4), 419−432.

(7) Liu, F.; Wang, Q.; Xu, P.; Andreazza, F.; Valbon, W. R.; Bandason, E.; Chen, M.; Yan, R.; Feng, B.; Smith, L. B.; Scott, J. G.; Takamatsu, G.; Ihara, M.; Matsuda, K.; Klimavicz, J.; Coats, J.; Oliveira, E. E.; Du, Y.; Dong, K. A dual-target molecular mechanism of pyrethrum repellency against mosquitoes. *Nat. Commun.* **2021**, *12* (1), 2553.

(8) Wang, Q.; Xu, P.; Andreazza, F.; Liu, Y.; Nomura, Y.; Duran, P.; Jiang, L.; Chen, M.; Takamatsu, G.; Ihara, M.; Matsuda, K.; Isaacs, R.; Oliveira, E. E.; Du, Y.; Dong, K. Identification of multiple odorant receptors essential for pyrethrum repellency in *Drosophila melanogaster*. *PLoS Genet.* **2021**, *17* (7), No. e1009677.

(9) Kikuta, Y.; Nakayama, K.; Katsuda, Y.; Hatanaka, A.; Yamada, G.; Mitsumori, T.; Matsuda, K. Variations of the *Tanacetum cinerariifolium* lipase influence its acyltransferase activity for pyrethrin synthesis. *Acta Hortic.* **2015**, *1073*, 153−155.

(10) Kikuta, Y.; Yamada, G.; Mitsumori, T.; Takeuchi, T.; Nakayama, K.; Katsuda, Y.; Hatanaka, A.; Matsuda, K. Requirement of catalytic-triad and related amino acids for the acyltransferase activity of *Tanacetum cinerariifolium* GDSL lipase/esterase TcGLIP for ester-bond formation in pyrethrin biosynthesis. *Biosci. Biotechnol. Biochem.* **2013**, *77* (9), 1822.

(11) Li, W.; Lybrand, D. B.; Xu, H.; Zhou, F.; Last, R. L.; Pichersky, E. A trichome-specific, plastid-localized *Tanacetum cinerariifolium* Nudix protein hydrolyzes the natural pyrethrin pesticide biosynthetic

intermediate trans-chrysanthemyl diphosphate. *Front. Plant Sci.* **2020**, *11*, 482.
(12) Li, W.; Zhou, F.; Pichersky, E. Jasmone hydroxylase, a key enzyme in the synthesis of the alcohol moiety of pyrethrin insecticides. *Plant Physiol.* **2018**, *177* (4), 1498−1509.
(13) Lybrand, D. B.; Xu, H.; Last, R. L.; Pichersky, E. How plants synthesize pyrethrins: Safe and biodegradable insecticides. *Trends Plant Sci.* **2020**, *25* (12), 1240−1251.
(14) Kikuta, Y.; Ueda, H.; Nakayama, K.; Katsuda, Y.; Ozawa, R.; Takabayashi, J.; Hatanaka, A.; Matsuda, K. Specific regulation of pyrethrin biosynthesis in *Chrysanthemum cinerariaefolium* by a blend of volatiles emitted from artificially damaged conspecific plants. *Plant Cell Physiol.* **2011**, *52* (3), 588−596.
(15) Ueda, H.; Kikuta, Y.; Matsuda, K. Plant communication: mediated by individual or blended VOCs? *Plant Signal. Behav.* **2012**, *7* (2), 222−226.
(16) Ueda, H.; Matsuda, K. VOC-mediated within-plant communications and nonvolatile systemic signals upregulate pyrethrin biosynthesis in wounded seedlings of *Chrysanthemum cinerariaefolium*. *J. Plant Interact.* **2011**, *6*, 89−91.
(17) Sugisaka, Y.; Aoyama, S.; Kumagai, K.; Ihara, M.; Matsuda, K. TcGLIP GDSL lipase substrate specificity co-determines the pyrethrin composition in *Tanacetum cinerariifolium*. *J. Agric. Food Chem.* **2022**, *70* (28), 8645−8652.
(18) Matsuo, N.; Sugisaka, Y.; Aoyama, S.; Ihara, M.; Shinoyama, H.; Hosokawa, M.; Kamakura, Y.; Tanaka, D.; Tanabe, Y.; Matsuda, K. Creating pyrethrin mimetic phosphonates as chemical genetics tools targeting the GDSL esterase/lipase TcGLIP to investigate pyrethrin biosynthesis. *J. Med. Chem.* **2023**, *66* (12), 7959−7968.
(19) Benjamini, Y.; Krieger, A. M.; Yekutieli, D. Adaptive linear step-up procedures that control the false discovery rate. *Biometrika* **2006**, *93*, 491−507.
(20) Morris, G. M.; Huey, R.; Lindstrom, W.; Sanner, M. F.; Belew, R. K.; Goodsell, D. S.; Olson, A. J. AutoDock4 and AutoDockTools4: Automated docking with selective receptor flexibility. *J. Comput. Chem.* **2009**, *30* (16), 2785−2791.
(21) Abraham, M. J.; Murtola, T.; Schulz, R.; Páll, S.; Smith, J. C.; Hess, B.; Lindahl, E. GROMACS: High performance molecular simulations through multi-level parallelism from laptops to supercomputers. *SoftwareX* **2015**, *1*−*2*, 19−25.
(22) He, X.; Man, V. H.; Yang, W.; Lee, T. S.; Wang, J. A fast and high-quality charge model for the next generation general AMBER force field. *J. Chem. Phys.* **2020**, *153* (11), 114502.
(23) Barca, G. M. J.; Bertoni, C.; Carrington, L.; Datta, D.; De Silva, N.; Deustua, J. E.; Fedorov, D. G.; Gour, J. R.; Gunina, A. O.; Guidez, E.; Harville, T.; Irle, S.; Ivanic, J.; Kowalski, K.; Leang, S. S.; Li, H.; Li, W.; Lutz, J. J.; Magoulas, I.; Mato, J.; Mironov, V.; Nakata, H.; Pham, B. Q.; Piecuch, P.; Poole, D.; Pruitt, S. R.; Rendell, A. P.; Roskop, L. B.; Ruedenberg, K.; Sattasathuchana, T.; Schmidt, M. W.; Shen, J.; Slipchenko, L.; Sosonkina, M.; Sundriyal, V.; Tiwari, A.; Galvez Vallejo, J. L.; Westheimer, B.; Włoch, M.; Xu, P.; Zahariev, F.; Gordon, M. S. Recent developments in the general atomic and molecular electronic structure system. *J. Chem. Phys.* **2020**, *152* (15), 154102.

https://doi.org/10.1021/acsomega.4c11003
ACS Omega 2025, 10, 19436−19443